Reactions of Laser-Ablated Ni, Pd, and Pt Atoms with Carbon Monoxide: Matrix Infrared Spectra and Density Functional Calculations on $M(CO)_n$ ($n = 1-4$), $M(CO)_n^-$ ($n = 1-3$), and $M(CO)_n^+$ ($n = 1-2$), (M = Ni, Pd, Pt)

Binyong Liang, Mingfei Zhou, and Lester Andrews*

Department of Chemistry, University of Virginia, Charlottesville, Virginia 22901

Received: October 12, 1999

Laser-ablated Ni, Pd, and Pt atoms have been reacted with CO molecules followed by condensation in excess neon at 4 K. Besides the neutral metal carbonyl species, metal carbonyl anions [$M(CO)_n^-$ ($n = 1-3$)] and cations [$Ni(CO)_n^+$ ($n = 1-4$), $Pd(CO)_n^+$ ($n = 1,2$), and $Pt(CO)_n^+$ ($n = 1-3$)] have been produced and identified. Doping with the CCl_4 electron trap increases cation and decreases anion absorptions and confirms the identification of the ionic species. The excellent agreement between observed bands and frequencies and isotopic frequency ratios from the DFT calculations supports the vibrational assignments and the identification of these metal carbonyl complexes.

I. Introduction

Binary transition-metal carbonyls are among the earliest known[1] and most commonly encountered organometallic compounds.[2] Metal carbonyl fragments are ubiquitous components of other organometallic compounds and larger metal clusters, and they are frequently invoked as active species in homogeneous catalytic cycles.[3] Moreover, the monocarbonyls are often considered as models for CO binding to the metal surface.[4,5] Nickel tetracarbonyl was the first metal carbonyl to be prepared,[1] and nickel group carbonyls are among the most studied metal carbonyls both experimentally by matrix-isolation spectroscopy[6] and theoretically.[7] The corresponding neutral $Pd(CO)_x$ and $Pt(CO)_x$ ($x = 1, 2, 3, 4$) carbonyls have been prepared using the matrix isolation technique, and their infrared spectra in argon and krypton matrices have been reported.[8−10] It is generally accepted that NiCO,[11−15] PdCO,[16] and PtCO[17] possess $^1\Sigma^+$ electronic states with linear geometries. The dicarbonyls have also been examined theoretically.[16] Finally, the vibrational spectra[18] and the force fields[19] of the tetracarbonyls have been reported.

On the other hand, comparatively less work has been done on the metal carbonyl cations and anions, especially their vibrational spectra. The photoelectron spectra (PES) of $Ni(CO)_n^-$ have given electron affinities and vibrational fine structure of neutral carbonyls.[20] Recently, the anion PES of $PdCO^-$ has been observed, and the electron affinity and CO vibrational frequency of PdCO have been deduced.[21] Collision-induced dissociation coupled with mass spectrometry have been employed to study sequential bond energies in $Ni(CO)_n^-$ ($n = 1-3$) and $Ni(CO)_n^+$ ($n = 1-4$).[22,23] Bond energies of the anions combined with the electron affinity data have been used to determine bond energies of the neutral species.[22] Finally, ionic Ni group carbonyls have received little theoretical attention; to our knowledge, only the mono- and dicarbonyl cations of Ni and Pd have been examined by theory.[24]

Recently, we reported argon matrix infrared spectra of $Ni(CO)_n^-$ ($n = 1-3$).[25] It will be interesting to determine the neon matrix interaction for the negative carbonyls and to find how Pd and Pt compare to the Ni counterparts. We will use the laser-ablation method to systematically study the reactions of Ni group atoms, cations, and electrons with CO in excess neon, and then use infrared spectroscopy coupled with CCl_4 doping to trap electrons[25] to identify the metal carbonyl neutrals, anions, and cations. We will also perform density functional theory (DFT) calculations to model these carbonyl species, including their vibrational analyses, ground state geometries, and bonding properties.

II. Experimental and Computational Methods

The experimental method for laser ablation and matrix isolation has been described in detail previously.[26−29] Briefly, the Nd:YAG laser fundamental (1064 nm, 10 Hz repetition rate with 10 ns pulse width) is focused to irradiate the rotating metal targets. Typically, low laser power (3−5 mJ/pulse) is used, which favors the stabilization of ionic species and minimizes metal cluster formation. Laser-ablated metal atoms are co-deposited with carbon monoxide (0.1%−0.4%) in excess neon onto a 4 K CsI cryogenic window at 2−4 mmol/h for 0.5−1 h. Carbon monoxide (Matheson) and isotopic $^{13}C^{16}O$ and $^{12}C^{18}O$ (Cambridge Isotopic Laboratories) and selected mixtures are used in different experiments. Fourier-transformed infrared (FTIR) spectra are recorded at 0.5 cm^{-1} resolution on a Nicolet 750 spectrometer with 0.1 cm^{-1} accuracy using a mercury cadmium telluride (MCTB) detector down to 400 cm^{-1}. Matrix samples are annealed at different temperatures, and selected samples are subjected to photolysis using a medium-pressure mercury lamp (240−580 nm) with the globe removed, or a tungsten lamp and applying optical filters when needed.

DFT calculations are performed on all of the proposed reaction products using the GAUSSIAN 94 program[30] and the hybrid B3LYP functional.[31] The 6-311+G* basis set is used for carbon, oxygen, and nickel,[32] and the LanL2DZ effective core potential is employed for palladium and platinum.[33] Natural bonding orbital (NBO) analyses are done for all of the nine monocarbonyls.[34]

III. Results and Discussion

A. Infrared Spectra and Assignments. Infrared spectra of laser-ablated Ni, Pd, and Pt atom, cation and electron reaction

10.1021/jp993646q CCC: $19.00 © 2000 American Chemical Society
Published on Web 04/04/2000

TABLE 1: Infrared Absorptions (cm^{-1}) from Reaction of Laser-Ablated Ni Atoms with CO in Excess Neon at 4 K

$^{12}C^{16}O$	$^{13}C^{16}O$	$^{12}C^{18}O$	$^{12}C^{16}O + ^{13}C^{16}O$	*R*(12/13)	*R*(16/18)	assignment
2347.6	2282.0	2312.5	2347.6, 2282.0	1.0288	1.0152	CO_2
2209.2	2159.9	2157.6		1.0228	1.0239	$Ni(CO)_2^+$ site
2206.5	2156.9	2156.0	2206.5, 2156.7	1.0230	1.0234	$NiCO^+$
2205.3	2156.1	2153.8	2205.3, 2165.9, 2156.1, 2223.8 (sym)	1.0228	1.0239	$Ni(CO)_2^+$
2192.4						$Ni(CO)_3^+$
2186.2		2135.2			1.0239	$Ni(CO)_3^+$
2176.2	2129.5	2124.9		1.0219	1.0241	$Ni(CO)_4^+$
2141.1	2093.6	2089.7	2141.1, 2093.6	1.0227	1.0246	CO
2091.4	2042.1	2046.9	2091.4, 2071.6, 2042.1	1.0241	1.0217	$Ni(CO)_2$ site
2089.7	2040.3	2045.3	2089.7, 2069.7, 2040.3	1.0242	1.0217	$Ni(CO)_2$
2056.3	2009.8	2009.2	2056.3, 2037.4, 2026.4, 2017.2, 2009.8	1.0231	1.0234	$Ni(CO)_4$
2026.9	1981.3	1980.1	2026.8, 2004.7, 1992.3, 1981.3	1.0230	1.0236	$Ni(CO)_3$ site
2025.0	1979.6	1978.3	2025.1, 2003.6, 1990.6, 1979.7	1.0229	1.0236	$Ni(CO)_3$
2006.6	1958.1	1965.4	2006.5, 1958.2	1.0248	1.0210	NiCO
1980.5	1936.4	1934.5	1980.6, 1953.7, 1936.4	1.0228	1.0238	$Ni(CO)_2$ site
1978.9	1934.7	1932.9	1978.9, 1951.9, 1934.7	1.0228	1.0238	$Ni(CO)_2$
1873.2	1832.5		1873.0, 1832.5	1.0221		Ni_xCO site
1870.5	1830.9	1830.6	1870.5, 1831.0	1.0216	1.0218	Ni_xCO
1867.7	1823.9	1824.9	1867.9, 1824.0, 1848.8, 1834.9	1.0240	1.0235	$Ni(CO)_3^-$ site
1864.7	1821.0	1823.4	1864.8, 1845.9, 1832.0, 1821.0	1.0240	1.0226	$Ni(CO)_3^-$
1860.6	1815.6	1821.0	1860.6, 1815.5	1.0248	1.0217	$NiCO^-$
1841.4	1798.5	1801.5	1841.1, 1798.6	1.0239	1.0221	Ni_xCO
1817.1	1774.8	1777.6	1817.2, 1790.0, 1774.9	1.0238	1.0222	$Ni(CO)_2^-$ site
1815.4	1773.2	1775.9	1815.4, 1788.2, 1773.7	1.0238	1.0222	$Ni(CO)_2^-$ site
1813.8	1771.6	1774.3	1813.8, 1786.8, 1771.7	1.0238	1.0223	$Ni(CO)_2^-$

TABLE 2: Infrared Absorptions (cm^{-1}) from Reaction of Laser-Ablated Pd Atoms with CO in Excess Neon at 4 K

$^{12}C^{16}O$	$^{13}C^{16}O$	$^{12}C^{18}O$	$^{12}C^{16}O + ^{13}C^{16}O$	*R*(12/13)	*R*(16/18)	assignment
2210.5	2161.1	2158.7	2210.5, 2169.8, 2161.1, 2225.0 (sym)	1.0228	1.0240	$Pd(CO)_2^+$
2206.4	2156.8	2155.4	2206.4, 2156.8	1.0230	1.0237	$Pd(CO)^+$
2074.6	2028.4	2026.0	2074.6, 2052.3, 2042.2, 2034.8, 2028.4	1.0228	1.0240	$Pd(CO)_4$
2068.2	2022.9	2019.0	2068.2, 2038.7, 2023.0, 2128.4 (sym)	1.0224	1.0244	$Pd(CO)_2$ site
2065.8	2020.5	2016.5	2065.8, 2036.3, 2020.5, 2125.2 (sym)	1.0224	1.0244	$Pd(CO)_2$
2064.7	2018.5			1.0229		$Pd(CO)_3$ site
2062.7	2016.7	2014.4	2062.7, 2037.4, 2026.0, 2016.8	1.0228	1.0240	$Pd(CO)_3$
2057.3	2009.6	2012.4	2057.3, 2009.6	1.0238	1.0224	PdCO site
2056.4	2008.7	2011.4	2056.4, 2008.7	1.0238	1.0224	PdCO
1909.0	1864.6	1868.2	1909.0, 1864.5	1.0238	1.0218	$Pd(CO)^-$
1902.7	1859.8	1859.3	1902.4, 1959.8	1.0231	1.0233	Pd_xCO
1878.8	1835.6	1836.4	1878.8, 1835.6	1.0235	1.0231	Pd_xCO
1872.2	1829.2	1831.9	1872.2, 1853.1, 1839.2, 1829.2	1.0235	1.0226	$Pd(CO)_3^-$
1870.1	1827.1	1828.8	1870.1, 1851.5, 1837.7, 1827.1	1.0235	1.0226	$Pd(CO)_3^-$ site
1834.3	1791.4	1794.6	1834.3, 1806.8, 1791.3	1.0239	1.0221	$Pd(CO)_2^-$ site
1832.3	1789.5	1792.9	1832.3, 1805.0, 1789.5	1.0239	1.0220	$Pd(CO)_2^-$

TABLE 3: Infrared Absorptions (cm^{-1}) from Reaction of Laser-Ablated Pt Atoms with CO in Excess Neon at 4 K

$^{12}C^{16}O$	$^{13}C^{16}O$	$^{12}C^{18}O$	$^{12}C^{16}O + ^{13}C^{16}O$	*R*(12/13)	*R*(16/18)	assignment
2210.3		2159.0	2210.3, 2173.5		1.0238	$Pt(CO)_2^+$
2207.9	2158.4	2156.7		1.0229	1.0237	$Pt(CO)_3^+$
2204.7		2156.7			1.0223	$PtCO^+$
2065.5	2014.9	2024.4	2065.5, 2014.9	1.0251	1.0203	PtCO
2064.7	2013.9	2023.4	2064.7, 2013.9	1.0252	1.0204	PtCO site
2058.1	2011.6	2010.9	2058.1, 2037.3, 2026.6, 2018.5, 2011.6	1.0231	1.0235	$Pt(CO)_4$
2056.2	2010.8	2007.5	2056.2, 2027.9, 2010.8	1.0226	1.0242	$Pt(CO)_2$ site
2053.2	2007.9	2004.7	2053.2, 2025.1, 2007.9	1.0226	1.0242	$Pt(CO)_2$
2046.0	1999.8	1999.7	2046.1, 2021.3, 2010.9, 1999.8	1.0231	1.0232	$Pt(CO)_3$ site
2044.0	1997.8	1997.1	2044.0, 2020.0, 2007.7, 1997.8	1.0231	1.0235	$Pt(CO)_3$
1896.3	1850.0	1858.7	1896.3, 1850.0	1.0250	1.0202	$PtCO^-$
1879.5	1835.3	1839.3		1.0241	1.0219	$Pt(CO)_3^-$ site
1875.8	1831.7	1835.7	1875.8, 1856.2, 1842.2, 1831.8	1.0241	1.0218	$Pt(CO)_3^-$
1844.0	1801.0	1804.6	1844.0, 1817.3, 1801.0	1.0238	1.0196	$Pt(CO)_2^-$

products with CO molecules in excess neon are displayed in Figures 1−9, and the absorption bands in different isotopic experiments are listed in Tables 1−3.

$Ni(CO)_n$ ($n = 1-4$). A strong absorption observed at 2006.6 cm^{-1} on deposition increases slightly on 6 K annealing but decreases during higher annealings. A band at 1978.9 cm^{-1} is also observed on deposition, and its intensity increases more than the 2006.6 cm^{-1} band during annealings. In mixed $^{12}CO/^{13}CO$ isotopic experiments, the 2006.6 cm^{-1} absorption shows a doublet feature, while the 1978.9 cm^{-1} band has a 1:2:1 triplet pattern. These two bands are assigned as the C−O stretching mode of NiCO and the antisymmetric C−O vibration of $Ni(CO)_2$, respectively. The 1978.9 cm^{-1} band exhibits a matrix site splitting at 1980.5 cm^{-1}. Compared to the NiCO and $Ni(CO)_2$ absorptions, the feature at 2025.0 cm^{-1} is weak on deposition, but increases steadily during annealings. This band

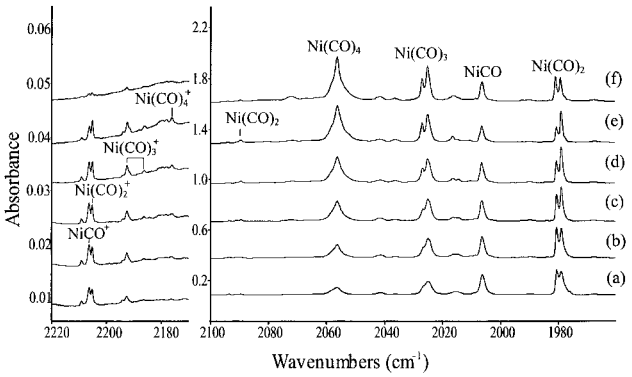

Figure 1. Infrared spectra in the 2220−2160 and 2100−1960 cm^{-1} regions for laser-ablated Ni co-deposited with 0.2% CO in neon at 4 K: (a) sample deposited for 30 min, (b) after 6 K annealing, (c) after 8 K annealing, (d) after 10 K annealing, (e) after 12K annealing, (f) after 240−580 nm photolysis.

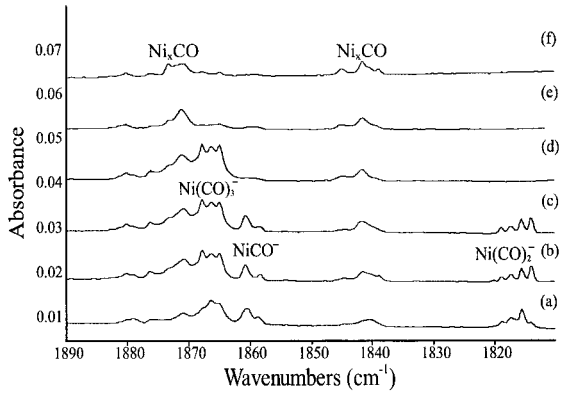

Figure 2. Infrared spectra in the 1890−1810 cm^{-1} region for laser-ablated Ni co-deposited with 0.2% CO in neon at 4 K: (a) sample deposited for 30 min, (b) after 8 K annealing, (c) after $\lambda > 630$ nm photolysis, (d) after $\lambda > 470$ nm photolysis, (e) after 240−580 nm photolysis, (f) after 10 K annealing.

has a 5:2:2:5 splitting pattern in the mixed $^{12}CO/^{13}CO$ isotopic experiment, which is characteristic of the doubly-degenerate mode of a trigonal species,[35] and accordingly, the 2025.0 cm^{-1} band is assigned to the doubly degenerate C−O stretching mode of $Ni(CO)_3$. The band at 2056.3 cm^{-1} is almost invisible on deposition and increases markedly in the annealings, and its splitting pattern in $^{12}CO/^{13}CO$ experiment is 8:2:3:2:8. It is assigned to the triply degenerate C−O stretching mode[35] of $Ni(CO)_4$. The isotopic counterparts and the mixed isotopic splittings of those bands are listed in Table 1. These results are in good agreement with the previous and recent argon matrix work; the $Ni(CO)_n$ bands show 12.2, 13.4, 7.8, and 5.1 cm^{-1} blue shifts in the neon matrix with $n = 1$, 2, 3, and 4, respectively.[25,36] Recent infrared spectra indicate that $Ni(CO)_2$ is bent in an argon matrix.[25,36] It is worth noting that the $Ni(CO)_2$ molecule is also bent in a neon matrix because a weak symmetric stretch is observed at 2089.7 cm^{-1}. In the $^{13}C^{16}O$ and $^{12}C^{18}O$ experiments, this band shifts to 2040.3 and 2045.3 cm^{-1}, respectively. In the mixed $^{12}CO/^{13}CO$ experiment, a 1:2:1 relative intensity triplet displays an intermediate band at 2069.7 cm^{-1} which is 4.7 cm^{-1} higher than the average of two pure isotopic bands. Correspondingly, the intermediate band of the antisymmetric stretch of $Ni(CO)_2$ is 4.9 cm^{-1} lower than the average of two pure isotopic bands, owing to the interaction between the two stretching modes in the lower symmetry $O^{13}C-Ni-^{12}CO$ molecule.

The symmetric modes at 2006.6 and 2089.7 cm^{-1} for NiCO and $Ni(CO)_2$ may be compared to the PES fine structure intervals[20] 1940 and 2100 ± 80 cm^{-1}; the weaker band in the $NiCO^-$ PES is more difficult to measure accurately.

$Pd(CO)_n$ ($n = 1-4$). Similar to $Ni(CO)_n$, the absorptions of $Pd(CO)_n$ are also observed and identified; the major difference is that the $Pd(CO)_n$ absorptions are more congested as also found in the thermal Pd atom work.[8,9] The new band observed at 2056.4 cm^{-1} on deposition is assigned to the C−O stretching mode of PdCO based on the doublet pattern in our mixed $^{12}CO/^{13}CO$ experiment. Another prominent band on deposition at 2065.8 cm^{-1} is assigned as the antisymmetric stretching mode of $Pd(CO)_2$, which shows a 1:2:1 splitting in our mixed $^{12}CO/^{13}CO$ experiment. The weaker $Pd(CO)_3$ and $Pd(CO)_4$ absorptions observed at 2062.7 and 2074.6 cm^{-1} become prominent bands during annealings (Figure 3). The annealing behaviors and the mixed isotopic splittings are very similar to those of $Ni(CO)_n$ ($n = 1-4$) bands.

This result is in agreement with the previous argon and krypton matrix work on PdCO, which reported bands at 2050

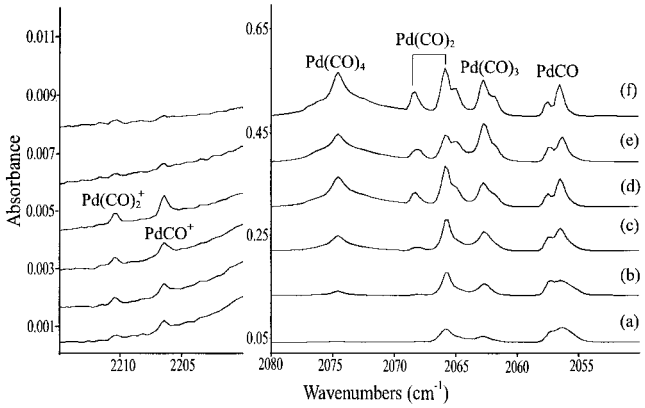

Figure 3. Infrared spectra in the 2215−2200 and 2080−2050 cm^{-1} regions for laser-ablated Pd co-deposited with 0.2% CO in neon at 4 K: (a) sample deposited for 30 min, (b) after 6 K annealing, (c) after 8 K annealing, (d) after 10 K annealing, (e) after 240−580 nm photolysis, (f) after 12 K annealing.

and 2044 cm^{-1}, respectively,[8,9] and with very recent argon matrix studies of Manceron et al.[36] who observed 2050.3 and 2044.2 cm^{-1} bands for PdCO. The PdCO fundamental is blue-shifted 6.1 and 12.2 cm^{-1} by the neon matrix. However, the 2140 ± 60 cm^{-1} fundamental for PdCO deduced from the photoelectron spectrum[21] of $PdCO^-$ is too high and probably suffers from accuracy of the weak fine structure band measurement. Our neon matrix observation at 2056.4 cm^{-1} is probably within 10 cm^{-1} of the true PdCO gas phase fundamental, which we predict at 2065 ± 5 cm^{-1}.

The interesting question here is again the structure of $Pd(CO)_2$. Both previous works observed $Pd(CO)_2$ at 2044 cm^{-1} (6 cm^{-1} *below* PdCO) and claimed that $Pd(CO)_2$ is a linear molecule because of the missing symmetric mode.[8,9] The geometry of this molecule might be linear because the pure isotopic symmetric stretching mode is not observed here. However, the bent structure for $Ni(CO)_2$ and the DFT calculation suggest a bent form. In our mixed $^{12}CO/^{13}CO$ experiment, a new band at 2125.2 cm^{-1} is observed in addition to the 1:2:1 relative intensity feature of the antisymmetric mode of $Pd(CO)_2$. This new band tracks with the 1:2:1 triplet bands and is assigned as the symmetric mode of $Pd(^{12}CO)(^{13}CO)$. The intermediate band of the triplet at 2036.3 cm^{-1} is 6.9 cm^{-1} lower than the average of two pure isotopic bands, which indicates $\nu_{sym} > \nu_{antisym}$. A similar spectrum was observed for $Rh(CO)_2$.[37] By analogy to the $Ni(CO)_2$ case, the weak 2125.2 cm^{-1} band should be about 7 cm^{-1} higher than the average of the two pure isotopic

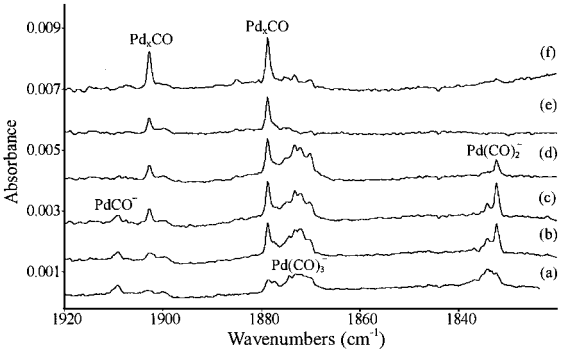

Figure 4. Infrared spectra in the 1920−1820 cm^{-1} region for laser-ablated Pd co-deposited with 0.2% CO in neon at 4 K: (a) sample deposited for 35 min, (b) after 8 K annealing, (c) after 10 K annealing, (d) after $\lambda > 630$ nm photolysis, (e) after $\lambda > 510$ nm photolysis, (f) after 12 K annealing.

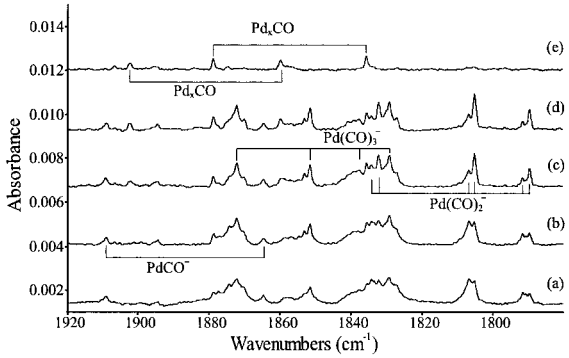

Figure 5. Infrared spectra in the 1920−1780 cm^{-1} region for laser-ablated Pd co-deposited with 0.15% ^{12}CO + 0.15% ^{13}CO in neon at 4 K: (a) sample deposited for 60 min, (b) after 6 K annealing, (c) after 8 K annealing, (d) after 10 K annealing, (e) after $\lambda > 470$ nm photolysis.

bands. On the basis of this information and the isotopic ratio from the DFT calculation, we estimate the symmetric modes of Pd(^{12}CO)$_2$ and Pd(^{13}CO)$_2$ to be near 2143 and 2093 cm^{-1}. Unfortunately, strong absorptions of ^{12}CO and ^{13}CO mask these regions. Hence, the geometry of this molecule is still an open question. Finally, the observation of Pd(CO)$_2$ at 9 cm^{-1} *above* PdCO in solid neon in contrast to 6 cm^{-1} *below* in solid argon and krypton[8,9] suggests that Pd(CO)$_2$ may be more bent in the more polar matrices. Such has been found for Fe(CO)$_2$ in solid neon and argon.[38]

The 2062.7 and 2074.6 cm^{-1} bands are assigned to Pd(CO)$_3$ and Pd(CO)$_4$ in solid neon are in good agreement with the argon matrix 2070 and 2058 cm^{-1} counterparts,[8,9] and the apparent 5 cm^{-1} blue shift in neon is reasonable.[37,38]

Pt(CO)$_n$ (n = 1−4). The absorptions of Pt(CO)$_n$ (n = 1−4) are similar to those for Ni(CO)$_n$ and Pd(CO)$_n$. The 2065.5 and 2064.7 cm^{-1} bands are assigned to the CO stretching mode of PtCO in two matrix sites. The absorptions at 2053.2, 2044.0, and 2058.1 cm^{-1} are assigned as antisymmetric modes of Pt(CO)$_2$, Pt(CO)$_3$, and Pt(CO)$_4$, respectively. The ^{12}CO/^{13}CO isotopic ratios for the Pt(CO)$_n$ (n = 1, 2, 3, 4) carbonyls are 1.0251, 1.0226, 1.0231, and 1.0231, respectively.

The early thermal Pt argon matrix work was complicated by congestion of all Pt(CO)$_n$ bands into a 10 cm^{-1} region; nevertheless, all four species were assigned with varying weight of evidence.[10] With 5% ^{12}CO and 5% ^{13}CO, a strong doublet at 2053.3 and 2006.9 cm^{-1} with three weaker intermediate components was assigned to tetrahedral Pt(CO)$_4$, and with more dilute 0.4% CO the strongest feature at 2052.0 cm^{-1} was attributed to PtCO. Unfortunately, the ^{12}CO/^{13}CO ratios are not accurate because of band overlap, which fortunately does not happen in solid neon as shown in Figure 8. Our PtCO band at 2065.5, 2064.7 cm^{-1} clearly forms a mixed isotopic doublet for a single CO group, and the high ^{12}CO/^{13}CO ratio (1.0251) is appropriate for this motion of C between Pt and O as observed for RhCO and IrCO.[37] (Manceron finds two sites for PtCO at 2056.8, 2057.9 cm^{-1} in solid argon.)[36] Our Pt(CO)$_2$ absorption forms a 1:2:1 triplet pattern at 2053.2, 2025.1, 2007.9 cm^{-1}, which is only slightly asymmetric. The neon matrix band at 2046.0, 2044.0 cm^{-1} is due to Pt(CO)$_3$; it shows one weaker intermediate component when two are expected for the antisymmetric mode of a trigonal species,[35] but band congestion may obscure another weak feature for mixed isotopic Pt(CO)$_3$. Our neon matrix band at 2058.1 cm^{-1} shows three possible weaker intermediate mixed isotopic features, as is expected for the triply-degenerate mode,[35] and is compatible with the argon matrix Pt(CO)$_4$ band at 2053.5 cm^{-1}. We believe that the neon

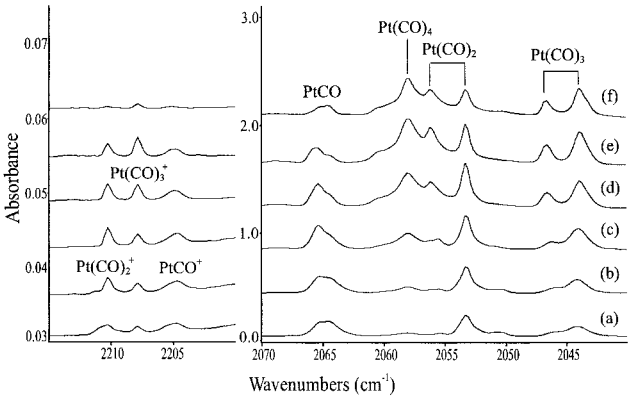

Figure 6. Infrared spectra in the 2215−2200 and 2070−2040 cm^{-1} regions for laser-ablated Pt co-deposited with 0.2% CO in neon at 4 K: (a) sample deposited for 40 min, (b) after 6 K annealing, (c) after 10 K annealing, (d) after 11 K annealing, (e) after 12 K annealing, (f) after 240−580 nm photolysis.

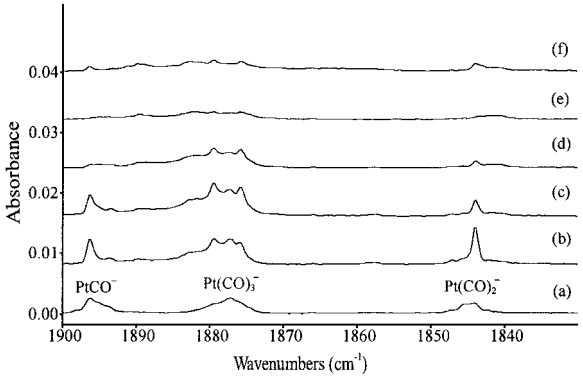

Figure 7. Infrared spectra in the 1900−1830 cm^{-1} region for laser-ablated Pt co-deposited with 0.2% CO in neon at 4 K: (a) sample deposited for 35 min, (b) after 8 K annealing, (c) after $\lambda > 470$ nm photolysis, (d) after $\lambda > 380$ nm photolysis, (e) after 240−580 nm photolysis, (f) after 12 K annealing.

matrix 2064.7 cm^{-1} and argon matrix[36] 2056.8 cm^{-1} assignments to PtCO are compatible, but our neon matrix data cast doubt on the argon matrix[10] identifications of Pt(CO)$_{2,3}$.

The symmetric stretching mode of Pt(CO)$_2$ is not observed in our experiments, which might simply mean this is a linear molecule. However, the DFT calculation again supports a bent structure for this molecule. The missing symmetric mode could be due to the low intensity or masking by other dominant peaks.

Compared to thermal metal atom reactions,[8−10,36] laser ablation also introduces cations and electrons into the reaction

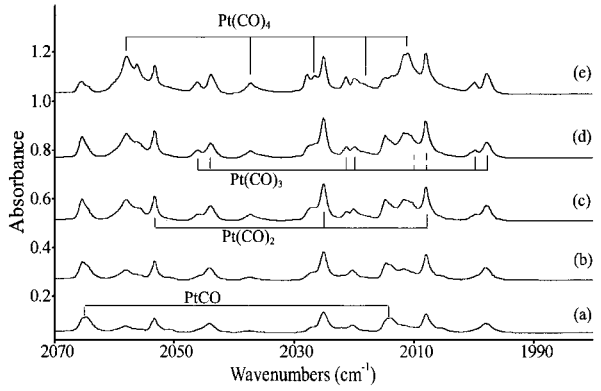

Figure 8. Infrared spectra in the 2070−1980 cm^{-1} region for laser-ablated Pt co-deposited with 0.15% ^{12}CO + 0.15%^{13}CO in neon at 4 K: (a) sample deposited for 45 min, (b) after 6 K annealing, (c) after 8 K annealing, (d) after 10 K annealing, (e) after 12 K annealing.

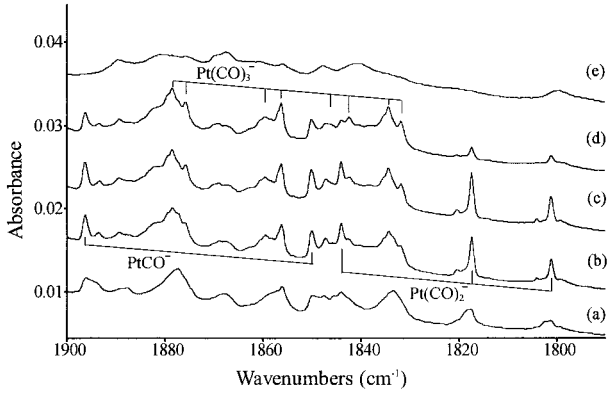

Figure 9. Infrared spectra in the 1900−1790 cm^{-1} region for laser-ablated Pt co-deposited with 0.15% ^{12}CO + 0.15% ^{13}CO in neon at 4 K: (a) sample deposited for 45 min, (b) after 8 K annealing, (c) after 10 K annealing, (d) after λ > 470 nm photolysis, (e) after 240−580 nm photolysis.

system. Additional weak bands in the low C−O stretching region (<1900 cm^{-1}) are observed in all three (Ni, Pd, Pt + CO) systems. These bands exhibit similar photosensitive behavior and are *almost eliminated* in CCl_4 doped experiments, so anion species must be considered.[25,37,38]

$Ni(CO)_n^-$ (n = 1, 2, 3). Three sets of weak photosensitive bands are observed on deposition at 1867.7 and 1864.7 cm^{-1}, at 1860.6 cm^{-1}, and at 1817.1, 1815.4, and 1813.8 cm^{-1}. The 1860.6 cm^{-1} band does not change during 6 and 8 K annealings but severely decreases during l0 and 12 K annealings and is destroyed with λ > 470 nm photolysis (Figure 2). The band has $^{13}C^{16}O$ and $^{12}C^{18}O$ counterparts at 1815.6 and 1821.0 cm^{-1}, with isotopic ratios of 1.0248 and 1.0217, and shows a doublet feature in the mixed $^{12}CO/^{13}CO$ experiment. This photosensitive band is assigned as $NiCO^-$. The 1817.1, 1815.4, and 1813.8 cm^{-1} band increases during annealings and is also destroyed by λ > 470 nm photolysis. In $^{13}C^{16}O$ and $^{12}C^{18}O$ experiments, this band shifts to 1774.8, 1773.2, and 1771.6 cm^{-1}, and to 1777.6, 1775.9, and 1774.3 cm^{-1}, respectively. The average isotopic ratios are 1.0238 ($^{12}CO/^{13}CO$) and 1.0222 ($C^{16}O/C^{18}O$). Each peak in this band shows a triplet feature in the mixed $^{12}CO/^{13}CO$ experiment. This photosensitive band is assigned as the C−O antisymmetric stretching mode of $Ni(CO)_2^-$. The 1864.7 and 1867.7 cm^{-1} band increases even more during annealings. However, λ > 470 nm photolysis does not destroy this band, but shorter wavelength photolysis (240−580 nm) does destroy it. This band has two weak intermediate components in the mixed $^{12}CO/^{13}CO$ experiment, which is appropriate for the degenerate stretching mode of a trigonal species,[25,35] and it is assigned to this C−O stretching mode of $Ni(CO)_3^-$.

These results are in excellent agreement with the recent argon matrix work.[25] The neon matrix blue-shifts the $Ni(CO)_n^-$ bands 13.6, 12.1, and 5.9 cm^{-1}, n = 1, 2, and 3, respectively.

$Pd(CO)_n^-$ (n = 1, 2, 3). The nickel carbonyl anions pave the way to identify the palladium carbonyl anions. Three photosensitive bands are formed in the low CO vibrational region on deposition: 1909.0 cm^{-1}, broad feature at 1872 cm^{-1} (splits to 1872.2 and 1870.1 cm^{-1} on late annealings), and 1834.3, 1832.3 cm^{-1}. The 1909.0 cm^{-1} band decreases slightly on annealing, and λ > 630 nm photolysis destroys this band (Figure 4d). In the $^{13}C^{16}O$ and $^{12}C^{18}O$ experiments, this band shifts to 1864.6 and 1868.2 cm^{-1}, respectively, and it shows a doublet feature in the mixed $^{12}CO/^{13}CO$ experiment. This band is assigned as the C−O stretching mode of the $PdCO^-$ anion. The 1834.3, 1832.3 cm^{-1} band increases during annealings, and photolysis (λ > 630 nm) decreases the band by half. The 12/13 and 16/18 isotopic ratios of this band are 1.0239 and 1.0220. In the mixed $^{12}CO/^{13}CO$ experiment, this band shows a characteristic 1:2:1 triplet feature. Therefore, this photosensitive band is assigned to the antisymmetric C−O stretching mode of $Pd(CO)_2^-$. The broad feature around 1872 cm^{-1} increases during annealing and increases on λ > 630 nm photolysis when $PdCO^-$ and $Pd(CO)_2^-$ disappear and decrease. However, shorter wavelength photolysis (510−630 nm) destroys this band. In the mixed $^{12}CO/^{13}CO$ experiment, the 1872.2, 1870.1 cm^{-1} band shows a quartet feature which is appropriate for a trigonal species.[25,35] Hence, this band is assigned to the antisymmetric C−O vibrational mode of $Pd(CO)_3^-$.

$Pt(CO)_n^-$ (n = 1, 2, 3). Similar to Ni and Pd experiments, three photosensitive bands are also observed in the low carbonyl vibrational region. The 1896.3 cm^{-1} band shows doublet feature in the mixed $^{12}CO/^{13}CO$ experiment (Figure 9), is destroyed by photolysis(λ > 380 nm), and is assigned as the C−O stretching mode of $PtCO^-$. The 1844.0 cm^{-1} absorption shows a sharp 1:2:1 feature in the mixed $^{12}CO/^{13}CO$ experiment and is assigned as the antisymmetric C−O stretching mode of $Pt(CO)_2^-$. The broad band near 1875 cm^{-1} is assigned to $Pt(CO)_3^-$, this assignment is supported by the quartet feature in the mixed $^{12}CO/^{13}CO$ experiment,[25,35] and it increases on λ > 470 nm photolysis at the expense of $PtCO^-$ and $Pt(CO)_2^-$.

Besides the anion bands in low CO vibrational region, some weak, photosensitive bands are also observed in the high C−O stretching region (>2140 cm^{-1}). In contrast to the anion species, the absorption intensities of these bands *increase* in the CCl_4 doping experiments. Hence, cation species are considered.[37,38]

$Ni(CO)_n^+$ (n = 1−4). The band at 2206.5 cm^{-1} is observed on deposition, increases during lower temperature annealings, and then decreases during higher temperature annealings. The 2205.3 cm^{-1} band is also observed on deposition with an intensity weaker than the 2206.5 cm^{-1} band, but after higher temperature annealings, this band is stronger than the 2206.5 cm^{-1} band. The 2192.5 cm^{-1} and another almost indiscernible 2186.2 cm^{-1} band are observed on deposition. They track together in all experiments, and their intensities increase steadily during annealings. The fourth band at 2176.2 cm^{-1} is weak on deposition and it increases on all annealings. All of these four sets of bands are destroyed by the medium-pressure mercury lamp photolysis (240−580 nm) (Figure 1f). These bands are assigned as nickel carbonyl cations: 2206.5 cm^{-1} is the C−O stretching mode of $NiCO^+$, 2205.3 cm^{-1} is the antisymmetric C−O stretching mode of $Ni(CO)_2^+$, and 2192.5 and 2186.2 cm^{-1} are assigned to the b_2 and a_1 C−O vibrational modes of the $Ni(CO)_3^+$ cation with a C_{2v} symmetry. The 2176.2 cm^{-1} band

is assigned to the e mode of the $Ni(CO)_4^+$ cation with a D_{2d} symmetry. The observed isotopic bands are listed in the Table 1. The mono- and dicarbonyl cation assignments are supported by the mixed $^{12}CO/^{13}CO$ experiment, which shows doublet feature at 2206.5 and 2156.0 cm^{-1} for $NiCO^+$, and an asymmetric 2:3:2 triplet feature at 2205.3, 2165.9, and 2156.1 cm^{-1} with a weaker associated 2223.8 cm^{-1} band for the symmetric stretching mode of the $Ni(^{12}CO)(^{13}CO)^+$ cation. The isotopic counterparts of bands of tri- and tetracarbonyl cations are difficult to identify, because some of the counterparts hide in the CO and CO aggregate bands which dominate around 2140 cm^{-1}. In the CCl_4-doped experiments, the absorptions of these nickel carbonyl cation bands increase while the anion bands are not observed. The CCl_4 molecule is well-known for its high electron capture cross section and resulting dissociative capture process giving CCl_3 and Cl^-. Hence, the assignments of the ions are supported by the CCl_4-doped experiments.[37,38] Finally, the observation of $NiCO^+$ absorption at 2205.3 cm^{-1} is consistent with the argon matrix work,[25] which gave a weak 2176.3 cm^{-1} absorption, 30.2 cm^{-1} lower, for $NiCO^+$.

Our DFT calculations are in very good agreement with the observations of these cations (scale factors 0.96−0.97). It is interesting to point out that the equilibrium geometries of $Ni(CO)_3^+$ and $Ni(CO)_4^+$ are C_{2v} and D_{2d} instead of D_{3h} and T_d. The observation of two C−O stretching modes for $Ni(CO)_3^+$ supports the calculated C_{2v} structure.

$Pd(CO)_n^+$ ($n = 1, 2$). Two photosensitive bands are observed in the high C−O vibrational region. The 2206.4 cm^{-1} band observed on deposition increases during annealings and decreases on photolysis. This band has $^{13}C^{16}O$ and $^{12}C^{18}O$ counterparts at 2156.8 and 2155.4 cm^{-1}. The weak 2210.5 cm^{-1} band also grows on annealing and decreases on photolysis, and $^{13}C^{16}O$ and $^{12}C^{18}O$ isotopic counterparts are at 2161.1 and 2158.7 cm^{-1}. In the mixed $^{12}CO/^{13}CO$ isotopic experiment, the 2206.4 cm^{-1} band shows a doublet feature, and the 2210.5 cm^{-1} band splits to a triplet with a fourth band at 2225.0 cm^{-1}. The 2206.4 cm^{-1} band is assigned as the C−O stretching mode of $Pd(CO)^+$, and the 2210.5 cm^{-1} band is the antisymmetric C−O stretching mode of $Pd(CO)_2^+$. The band at 2225.0 cm^{-1} in the mixed isotopic experiment is the symmetric stretching mode of $Pd(^{12}CO)(^{13}CO)^+$. In the CCl_4-doped experiment, both bands increase while the anion bands are absent from the 1820−1920 cm^{-1} region.[37,38]

$Pt(CO)_n^+$ ($n = 1, 2, 3$). Three bands are observed at 2210.3, 2207.9, and 2204.7 cm^{-1} in the high C−O vibrational region on deposition. With 0.1% CO/Ne, the 2204.7 cm^{-1} band is the strongest, but with 0.2% CO/Ne, the 2210.3 cm^{-1} band becomes the strongest (Figure 6). In the 0.2% CO experiments, the 2204.7 cm^{-1} band shows only a small increase after 6 K annealing, then no change after 10 K annealing, and finally decreases after 11 and 12 K annealings. The 2210.3 cm^{-1} band increases by half after 6 K annealing, increases again after 10 K annealing, but the intensity of this band decreases after 11 and 12 K annealings. The 2207.9 cm^{-1} band is the weakest band on deposition, but it keeps increasing on annealings; after 12 K annealing, this band is the strongest among the three. Photolysis after the annealings almost destroys the three bands. The three bands at 2210.3, 2207.9, and 2204.7 cm^{-1} are assigned as $Pt(CO)_2^+$, $Pt(CO)_3^+$, and $PtCO^+$, respectively. Some of isotopic counterparts and intermediate bands in mixed isotopic experiments are not observable due to the dominant CO and aggregate absorptions in this region. As expected, in the 0.02% CCl_4-doped experiment, these three bands increase by at least half again while the anion products are absent.

Other Absorptions. In Ni and Pd + CO reactions, several extra bands are observed in the low C−O stretching region or the metal carbonyl anion region. In the Ni + CO experiment, absorptions at 1870.5 and 1841.4 cm^{-1} are observed on deposition, increase during annealing, and *are not* eliminated by photolysis. When higher laser power is employed, the absorption intensities of both bands increase, but metal carbonyl anions decrease with higher laser power. Both bands show isotopic shifts in ^{13}CO and $C^{18}O$ experiments, and both become doublets in the mixed $^{12}CO/^{13}CO$ isotopic experiments. Therefore, Ni cluster monocarbonyls are reasonable candidates for those absorptions. The 1841.4 cm^{-1} absorption is stronger than the 1870.5 cm^{-1} absorption on deposition, but grows slower than the 1870.5 cm^{-1} absorption on annealings. We are inclined to assign tentatively the 1841.4 cm^{-1} absorption as Ni_2CO, and the 1870.5 cm^{-1} absorption as Ni_3CO. The absorption at 1873.2 cm^{-1} is a matrix site of the 1870.5 cm^{-1} absorption. Similar to the Ni + CO experiment, there are also two bands observed in the Pd + CO experiment. On the basis of the similar behaviors as the Ni_2CO and Ni_3CO in the Ni + CO experiment, the 1878.8 and 1902.7 cm^{-1} bands are tentatively assigned as Pd_2CO and Pd_3CO.

B. Calculations: Theoretical Considerations. The results of DFT calculations are listed in Tables 4−8. We have calculated different geometries and different spin multiplicities for these species. Only the most stable ones (the lowest energy, and no negative vibrational frequencies) are listed.

As a first step, reproducing the correct ground state of the metal atoms is a difficult task. From our knowledge in general chemistry, the ground state configuration of Ni atom is [Ar]-$3d^84s^2$, Pd is [Kr]4d,[10] and Pt is [Xe]$4f^{14}5d^96s^1$. In our DFT calculation (B3LYP functional, 6-311+G* basis set on C, O, and Ni or LANL2DZ on Pd and Pt), the ground states of Pd and Pt are reproduced, but Ni is calculated to have the [Ar]-$3d^94s^1$ ground state configuration, as found by other DFT calculations.[11,14] For CO, the calculated bond length is 1.128 Å and the harmonic vibrational frequency is 2211.8 cm^{-1}. These results are in excellent agreement with the experimental values,[40] CO bond length, 1.128 Å, and the harmonic vibrational frequency (ω_e), 2169.8 cm^{-1}.

The binding energies of the carbonyls are listed in Tables 4−6. All of those values are positive, which means that adding CO to unsaturated carbonyls are exothermic reactions. During deposition, excess CO is condensed in the neon matrix so excess CO can react with unsaturated metal carbonyls to produce higher order carbonyls if enough energy is available to overcome any barriers. In our annealing experiments, the intensities of the higher order carbonyl absorptions increase while the lower order carbonyls decrease. These observations are well supported by the calculations. The previous experimental bond energy data of $(CO)_nNi-CO$ ($n = 0, 1, 2$) are 40.5 ± 5.8, 47.1 ± 5.8, and 28.3 ± 2.3 kcal/mol,[22] $(CO)_nNi^--CO$ ($n = 1,2$) are 43.4 ± 5.8 and 38.5 ± 2.3 kcal/mol,[22] $(CO)_nNi^+-CO$ ($n = 1,2,3$) are 40.4 ± 2.5, 22.6 ± 1.4, and 18.4 ± 0.7 kcal/mol.[23] Since the zero-point energy (ZPE) and basis set superposition error (BSSE) only account for several kcal/mol, we have not done these corrections. Nevertheless, our "raw" calculation results for binding energies of $(CO)_nNi-CO$ ($n = 0, 1, 2$) 32.9, 40.8, and 27.4 kcal/mol, $(CO)_nNi^--CO$ ($n = 1,2$) 43.0 and 39.3 kcal/mol, and $(CO)_nNi^+-CO$ ($n = 1,2,3$) 37.5, 21.0, and 16.8 kcal/mol are close (within 10%−20%) to the experimental data.

Electron affinities (EA) of monocarbonyls are also listed in Tables 4−6. Combined with the binding energies, we can get the EAs of $Ni(CO)_n$ ($n = 1, 2, 3$) as 13.8, 16.0, and 27.9 kcal/

TABLE 4: Ground Electronic States, Equilibrium Geometries, Binding Energies, and Frequencies Calculated (B3LYP/6-311+G*) for the Ni Carbonyls

species	electronic state	point group	binding energy (kcal/mol) [a]	geometry (Å, deg)	frequencies (intensity)[g]
CO	$^1\Sigma^+$	$C_{\infty v}$		C−O: 1.128	2211.8(89)
NiCO	$^1\Sigma^+$	$C_{\infty v}$	32.9[b]	Ni−C: 1.685, C−O: 1.151	345.0(9 × 2), 585.9(5), 2083.6(745)
$Ni(CO)_2$	$^1A_1$	C_{2v}	40.8	Ni−C: 1.781, C−O: 1.141, ∠CNiC: 150.7, ∠NiCO: 173.7	426.2(4), 450.6(0), 496.0(153), 2073.3(2137), 2162.7(72)
$Ni(CO)_3$	$^1A_1'$	D_{3h}	27.4	Ni−C: 1.819, C−O: 1.139	484.0(5 × 2), 2094.5(1378 × 2), 2173.1(0)
$Ni(CO)_4$	$^1A_1$	T_d	20.3	Ni−C: 1.846, C−O: 1.138	464.3(0), 2113.3(1032 × 3), 2186.2(0)
$NiCO^-$	$^2\Sigma^+$	$C_{\infty v}$	−13.8[c]	Ni−C: 1.691, C−O: 1.172	224.4(87 × 2), 573.2(0), 1937.6(1066)
$Ni(CO)_2^-$	$^2\Pi_u$	$D_{\infty h}$	43.0	Ni−C: 1.766, C−O: 1.175	402.2(17), 448.5(0), 458.5(1), 1867.3(2960), 1936.0(0)
$Ni(CO)_3^-$	$^2A_2''$	D_{3h}	39.3	Ni−C: 1.784, C−O: 1.166	514.0(9 × 2), 1913.4(2266 × 2), 1997.7(0)
$NiCO^+$	$^2\Sigma^+$	$C_{\infty v}$	175.1[d]	Ni−C: 1.896, C−O: 1.118	294.5(0 × 2), 378.0(3), 2294.3(178)
$Ni(CO)_2^+$	$^2\Sigma_g^+$	$D_{\infty h}$	37.5	Ni−C: 1.931, C−O: 1.118	379.4(28), 405.6(3 × 2), 2279.6(545), 2308.5(0)
$Ni(CO)_3^+$	$^2A_1$	C_{2v}	21.0	Ni−C′: 1.961, C′−O′: 1.121, Ni−C: 1.954, C−O: 1.119, ∠CNiC: 154.9, ∠NiCO: 179.9[e]	387.7(4), 400.0(8), 2260.7(296), 2265.1(538), 2292.8(1)
$Ni(CO)_4^+$	$^2B_2$	D_{2d}	16.8	Ni−C: 1.982, C−O: 1.121, ∠CNiC:[f] 129.0, ∠NiCO: 175.8	408.2(0), 2247.8(280), 2251.1(434 × 2), 2280.0(0)

[a] Binding energies refer to the reactions: $Ni(CO)_{n-1}^q + CO \rightarrow Ni(CO)_n^q$, without ZPE and BSSE corrections. [b] The ground state of Ni atom is calculated as $[Ar]3d^94s^1$ configuration. [c] Relative energy compared to NiCO (−EA of NiCO). [d] Relative energy compared to NiCO (IE of NiCO). [e] C′ and O′ are on the C_2 axis. C and O refer to others. [f] These two carbon atoms are in one dihedral plane. [g] Highest frequencies listed, no negative roots for any frequencies.

TABLE 5: Ground Electronic States, Equilibrium Geometries, Binding Energies, and Frequencies Calculated for the Pd Carbonyls[a]

species	electronic state	point group	binding energy (kcal/mol)[b]	geometry (Å, deg)	frequencies (intensity)[g]
PdCO	$^1\Sigma^+$	$C_{\infty v}$	41.3	Pd−C: 1.873, C−O: 1.143	242.4(7 × 2), 445.3(12), 2112.9(629)
$Pd(CO)_2$	$^1A_1$	C_{2v}	29.7	Pd−C: 1.965, C−O: 1.135, ∠CPdC: 162.5, ∠PdCO: 176.2	321.0(3), 366.0(130), 383.0(0), 2121.1(1826), 2190.3(28)
$Pd(CO)_3$	$^1A_1'$	D_{3h}	11.6	Pd−C: 2.020, C−O: 1.135	413.6(2 × 2), 2120.2(1184 × 2), 2174.9(0)
$Pd(CO)_4$	$^1A_1$	T_d	4.7	Pd−C: 2.070, C−O: 1.134	369.2(2), 2129.9(901 × 3), 2183.0(0)
$PdCO^-$	$^2A'$	C_s	−10.8[c]	Pd−C: 1.873, C−O: 1.168, ∠PdCO: 154.3	203.9(143), 478.4(38), 1914.2(1913)
$Pd(CO)_2^-$	$^2\Pi_u$	$D_{\infty h}$	32.9	Pd−C: 1.935, C−O: 1.169	345.5(11), 347.4(17), 408.0(0), 1887.5(3436), 1943.4(0)
$Pd(CO)_3^-$	$^2A_2''$	D_{3h}	19.3	Pd−C: 1.976, C−O: 1.161	448.5(17 × 2), 1921.5(2523 × 2), 1990.2(0)
$PdCO^+$	$^2\Sigma^+$	$C_{\infty v}$	201.5[d]	Pd−C: 1.996, C−O: 1.118	282.4(0 × 2), 327.3(4), 2287.4(174)
$Pd(CO)_2^+$	$^2\Sigma_g^+$	$D_{\infty h}$	32.6	Pd−C: 2.061, C−O: 1.117	301.7(0), 398.1(5 × 2), 2285.6(431), 2311.3(0)
$Pd(CO)_3^+$	$^2A_1$	C_{2v}	15.2	Pd−C: 2.088, C−O: 1.119, Pd−C′: 2.138, C′−O′: 1.120 ∠CPdC: 166.1, ∠PdCO: 178.5[e]	337.5(3), 384.4(7), 2265.7(203), 2267.8(478), 2291.3(0)
$Pd(CO)_4^+$	$^2B_2$	D_{2d}	10.5	Pd−C: 2.174, C−O: 1.121, ∠CPdC:[f] 154.5, ∠PdCO: 178.4	324.3(0), 2253.9(53), 2254.4(427 × 2), 2276.9(0)

[a] DFT calculation: B3LYP functional, 6-311+G* basis set on C and O, LANL2DZ basis set and ECP on Pd. The ground state of Pd atom is calculated as $[Kr]4d^{10}4s^0$ configuration. [b] Binding energies refer to the reactions: $Pd(CO)_{n-1}^q + CO \rightarrow Pd(CO)_n^q$, without ZPE and BSSE corrections. [c] Relative energy compared to PdCO (−EA of PdCO). [d] Relative energy compared to PdCO (IE of PdCO). [e] C′ and O′ are on the C_2 axis. C and O refer to others. [f] These two carbon atoms are in one dihedral plane. [g] Highest frequencies listed, no negative frequencies.

mol. The experimental data are 18.5 ± 0.3, 14.8 ± 0.3, and 24.8 ± 0.3 kcal/mol.[20] Similarly, the ionization energies (IE) of the $Ni(CO)_n$ ($n = 1-4$) are calculated as 175.1, 178.4, 184.8, and 188.3 kcal/mol, and the experimental data are 168.3 ± 6.7, 179.6 ± 5.1, 177.3 ± 5.8, and 188.4 ± 5.3 kcal/mol.[22] Both EA and IE values are close to the experimental measurements. Recently, the EA of PdCO has been deduced in anion photoelectron spectroscopy,[21] and our value (10.8 kcal/mol) is close to the experimental value (13.9 ± 0.2 kcal/mol). Although there is concern about the accuracy of DFT anion energies for the calculation of electron affinity,[39] the present B3LYP calculations for EA's and IE's of $Ni(CO)_n$ are within 10% of experimental measurements except for the EA of NiCO (25% too low).

The C−O stretching modes largely depend on the strengths of the C−O bonds. The bond lengths of C−O units can be used to reflect the strengths of the C−O bonds. In all these three metal carbonyls, the cations have shorter C−O bonds than neutrals, while the neutrals have shorter C−O bonds than anions. As a result, the C−O vibrational frequencies (stretching modes) of the cations are higher than neutrals, and those of neutrals are higher than anions. The calculated frequencies as well as experimental values have shown this trend. The detailed comparison between calculated and experimental values is listed in Table 7. The average of scale factors is 0.971 ± 0.007. The B3LYP functional is well-known for higher frequencies, and the scale factor for this method is generally around 0.95−1.00.[41] On the other hand, the calculated harmonic frequencies should be larger than the experimental fundamental modes which include anharmonicity factors. Matrix shifts contribute to the difference between calculated and experimental values. If we take CO as our standard, which gives scale factor 0.968, the average scale factor of the carbonyl complexes is quite acceptable.

The isotopic frequency ratios of these C−O vibrational modes are well-defined by the calculations (Table 7). They give strong support in assigning these bands, especially when the C−O stretching vibrations of Pd and Pt carbonyl neutrals are very congested.

In the case of CO bonded to cation center, such "nonclassical" carbonyls with frequencies higher than CO itself have been

TABLE 6: Ground Electronic States, Equilibrium Geometries, Binding Energies, and Frequencies Calculated for the Pt Carbonyls[a]

species	electronic state	point group	binding energy (kcal/mol)[b]	geometry (Å, deg)	frequencies (intensity)[g]
PtCO	$^1\Sigma^+$	$C_{\infty v}$	66.6	Pt−C: 1.781, C−O: 1.148	404.7(2 × 2), 590.3(5), 2121.4(659)
$Pt(CO)_2$	$^1A_1$	C_{2v}	43.5	Pt−C: 1.909, C−O: 1.138, ∠CPtC: 157.1, ∠PtCO: 171.5	452.4(0), 463.3(0), 520.5(0), 2108.9(1934), 2195.4(64)
$Pt(CO)_3$	$^1A_1'$	D_{3h}	12.1	Pt−C: 1.956, C−O: 1.139	507.9(14 × 2), 2104.2(1299 × 2), 2165.9(0)
$Pt(CO)_4$	$^1A_1$	T_d	3.7	Pt−C: 1.996, C−O: 1.137	472.6(18), 2114.5(1013 × 3), 2174.2(0)
$PtCO^-$	$^2A'$	C_s	−23.6[c]	Pt−C: 1.820, C−O: 1.172, ∠PtCO: 165.9	191.4(137), 547.8(26), 1935.4(1132)
$Pt(CO)_2^-$	$^2\Pi_u$	$D_{\infty h}$	41.5	Pt−C: 1.901, C−O: 1.172	406.0(0), 489.4(1), 501.5(0), 1896.1(2898), 1975.5(0)
$Pt(CO)_3^-$	$^2A_2''$	D_{3h}	20.7	Pt−C: 1.923, C−O: 1.165	533.0(46 × 2), 1925.9(2135 × 2), 1994.5(0)
$PtCO^+$	$^2\Sigma^+$	$C_{\infty v}$	216.5[d]	Pt−C: 1.861, C−O: 1.124	383.3(0 × 2), 492.1(18), 2262.2(321)
$Pt(CO)_2^+$	$^2\Sigma_g^+$	$D_{\infty h}$	47.9	Pt−C: 1.984, C−O: 1.119	421.1(0), 504.7(12 × 2), 2262.2(744), 2315.4(0)
$Pt(CO)_3^+$	$^2A_1$	C_{2v}	24.2	Pt−C′: 2.004, C′−O′: 1.122, Pt−C: 1.998, C−O: 1.121, ∠CPtC: 163.0, ∠PtCO: 178.2 [e]	436.7(8), 494.8(15), 2243.1(790), 2245.2(350), 2286.1(3)
$Pt(CO)_4^+$	$^2B_2$	D_{2d}	11.4	Pt−C: 2.030, C−O: 1.124, ∠CPtC:[f] 153.3, ∠PtCO: 173.6	433.4(14), 2212.5(870 × 2), 2217.0(99), 2252.9(0)

[a] DFT calculation: B3LYP functional, 6-311+G* basis set on C and O, LANL2DZ basis set and ECP on Pt. The ground state of Pt atom is calculated as $[Xe]4f^{14}5d^96s^1$ configuration. [b] Binding energies refer to the reactions: $Pt(CO)_{n-1}^q + CO \rightarrow Pt(CO)_n^q$, without ZPE and BSSE corrections. [c] Relative energy compared to PtCO (−EA of PtCO). [d] Relative energy compared to PtCO (IE of PtCO). [e] C′ and O′ are on the C_2 axis. C and O refer to others. [f] These two carbon atoms are in one dihedral plane. [g] Highest frequencies listed, no negative roots for any frequencies.

TABLE 7: Comparison of Computed and Experimental C−O Stretching Modes of the Ni Group Carbonyls[a]

species	stretching mode	computed			experimental			scale factor (exp/comp)
		freq (cm^{-1})	*R*(12/13)	*R*(16/18)	freq (cm^{-1})	*R*(12/13)	*R*(16/18)	
NiCO	σ	2083.6	1.0248	1.0217	2006.6	1.0248	1.0210	0.963
$Ni(CO)_2$	b_2	2073.3	1.0232	1.0241	1978.9	1.0228	1.0238	0.955
	a_1	2162.7	1.0244	1.0224	2089.7	1.0242	1.0217	0.966
$Ni(CO)_3$	e′	2094.5	1.0233	1.0239	2025.0	1.0229	1.0236	0.967
$Ni(CO)_4$	t_2	2113.3	1.0233	1.0239	2056.3	1.0231	1.0234	0.973
$NiCO^-$	σ	1937.6	1.0250	1.0212	1860.6	1.0248	1.0217	0.960
$Ni(CO)_2^-$	σ_u	1867.3	1.0242	1.0226	1813.8	1.0238	1.0223	0.971
$Ni(CO)_3^-$	e′	1913.4	1.0244	1.0227	1864.7	1.0240	1.0226	0.975
$NiCO^+$	σ	2294.3	1.0234	1.0238	2206.5	1.0230	1.0234	0.962
$Ni(CO)_2^+$	σ_u	2279.6	1.0231	1.0243	2205.3	1.0228	1.0239	0.967
$Ni(CO)_3^+$	a_1	2260.7	1.0231	1.0243	2186.2		1.0239	0.967
	b_2	2265.1	1.0230	1.0244	2192.4			0.968
$Ni(CO)_4^+$	e	2247.8	1.0230	1.0245	2176.2			0.968
PdCO	σ	2112.9	1.0239	1.0230	2056.4	1.0238	1.0224	0.973
$Pd(CO)_2$	b_2	2121.1	1.0229	1.0246	2065.8	1.0224	1.0244	0.974
$Pd(CO)_3$	e′	2120.2	1.0230	1.0244	2062.7	1.0228	1.0240	0.973
$Pd(CO)_4$	t_2	2129.9	1.0229	1.0245	2074.6	1.0228	1.0240	0.974
$PdCO^-$	a′	1914.2	1.0239	1.0231	1909.0	1.0238	1.0218	0.997
$Pd(CO)_2^-$	σ_u	1887.5	1.0240	1.0228	1832.3	1.0239	1.0220	0.971
$Pd(CO)_3^-$	e′	1921.5	1.0238	1.0233	1872.2	1.0235	1.0226	0.974
$PdCO^+$	σ	2287.4	1.0232	1.0240	2206.4	1.0230	1.0237	0.965
$Pd(CO)_2^+$	σ_u	2285.6	1.0230	1.0244	2210.5	1.0228	1.0240	0.967
$Pd(CO)_3^+$	b_2	2267.8	1.0230	1.0245				
$Pd(CO)_4^+$	e	2254.4	1.0229	1.0246				
PtCO	σ	2121.4	1.0253	1.0209	2065.5	1.0251	1.0203	0.974
$Pt(CO)_2$	b_2	2108.9	1.0232	1.0240	2053.2	1.0226	1.0242	0.974
$Pt(CO)_3$	e′	2104.2	1.0234	1.0238	2044.0	1.0231	1.0235	0.971
$Pt(CO)_4$	t_2	2114.5	1.0233	1.0240	2058.1	1.0231	1.0235	0.973
$PtCO^-$	a′	1935.4	1.0251	1.0213	1896.3	1.0250	1.0202	0.980
$Pt(CO)_2^-$	σ_u	1896.1	1.0243	1.0225	1844.0	1.0238	1.0196	0.973
$Pt(CO)_3^-$	e′	1925.9	1.0244	1.0224	1875.8	1.0241	1.0218	0.974
$PtCO^+$	σ	2262.2	1.0241	1.0227	2204.7		1.0223	0.975
$Pt(CO)_2^+$	σ_u	2262.2	1.0230	1.0244	2210.3		1.0238	0.977
$Pt(CO)_3^+$	b_2	2243.1	1.0231	1.0243	2207.9	1.0229	1.0237	0.984
$Pt(CO)_4^+$	e	2212.5	1.0230	1.0244				
CO	σ	2211.8	1.0228	1.0248	2141.1	1.0227	1.0246	0.968

[a] There is no single negative mode in the vibrational frequencies calculated for all of these molecules.

explained by electrostatic effects.[42] The agreement of $NiCO^+$, $PdCO^+$, and $PtCO^+$ frequencies within 2 cm^{-1} shows that electrostatic effects dominate here, even more so than predicted by the B3LYP calculations, which suggest a 32 cm^{-1} spread for these carbonyl cation species.

The bonding properties of monocarbonyls always receive extra attention because they are considered as the models of the CO binding to the metal surface.[13−17] In our calculations, all the monocarbonyls are linear, except $PdCO^-$ and $PtCO^-$ which are calculated to be bent by both DFT/B3LYP and BP86

TABLE 8: Natural Bonding Orbital Analyses of Ni Group Monocarbonyls

species	conformn of Ni	BO of CO	species	conformn of Pd	BO of CO	species	conformn of Pt	BO of CO
NiCO	$3d^{9.37}4s^{0.53}$	2.80	PdCO	$4d^{9.53}5s^{0.40}$	2.84	PtCO	$5d^{9.17}6s^{0.91}$	2.77
$NiCO^+$	$3d^{8.96}4s^{0.13}$	2.95	$PdCO^+$	$4d^{9.05}5s^{0.12}$	2.94	$PtCO^+$	$5d^{8.89}6s^{0.36}$	2.87
$NiCO^-$	$3d^{9.25}4s^{1.21}$	2.73	$PdCO^-$	$4d^{9.40}5s^{1.06}$	2.76	$PtCO^-$	$5d^{9.12}6s^{1.35}$	2.67

functionals. The description of the bonding of CO to transition metals usually involves the mechanism of σ donation and π back-donation. To address this bonding mechanism, we have applied natural bonding orbital (NBO) analysis[34] to the monocarbonyls, and results are listed in Table 8.

First, the cations have higher C−O bond orders than neutrals, and neutrals have higher C−O bond orders than anions. Again, this shows us that C−O stretching frequencies have the order cations > neutrals > anions, as found for other transition metals.[37,38]

Second, the different configurations of metal atoms in anions, cations, or neutrals can be used to explain the different geometries. Anions have the largest s electron component, while neutrals and cations have smaller s character. The σ donation in carbonyls is always explained as the 5σ electrons of CO molecule donating to valence s orbital (or sd_σ hybridized orbital) of metal atom, while π back-donation is the valence d_π electrons of metal atom donating to $2\pi^*$ orbital of CO. The electrons in valence s orbital (or sd_σ hybridized orbital) of metal atom can substantially decrease the M−CO bond strength because of the repulsion between the metal s electrons and the CO 5σ electrons. To relax this repulsion, it is energy wise for metal atom to undergo s to d electron promotion. In the NBO analyses, this promotion is confirmed by a comparatively smaller s component, but a larger d component in the metal valence electron configurations. In carbonyl anions, the metal atom has larger valence s character than in the neutrals and cations, and hence, the repulsive forces between metal s electrons and CO 5σ electrons are larger. Because the 5σ orbital of CO does not point directly toward the metal in bent geometry, the σ repulsion is smaller. This repulsion probably acts as a driving force for bending in the Pd and Pt carbonyl anions. The geometric differences between linear $NiCO^-$ and the other two carbonyl anions are not easy to understand because in our NBO analysis, Ni atom shows similar larger valence s component as Pd and Pt atoms in their monocarbonyl anions. Additional theoretical calculations are necessary to clarify this problem.

IV. Conclusions

Laser-ablated Ni, Pd, and Pt atoms have been reacted with CO molecules during condensation in a neon matrix at 4 K. Through annealing, photolysis, and isotopic substitution experiments, metal carbonyl anions [$M(CO)_n^-$ ($n = 1-3$)] and cations [$Ni(CO)_n^+$ ($n = 1-4$); $Pd(CO)_n^+$ ($n = 1,2$); $Pt(CO)_n^+$ ($n = 1-3$)], as well as neutrals [$M(CO)_n$ ($n = 1-4$)] have been identified. Evidence for nonlinear geometries of dicarbonyls [$M(CO)_2$] is provided. The CCl_4-doped experiments are used to confirm the identification of the ionic species.[25,37,38] Tentative assignments for Ni and Pd cluster monocarbonyls [M_xCO, ($x = 2, 3$; M = Ni, Pd)] are also made.

The excellent agreement between experiment results and the frequencies and isotopic frequency ratios from the DFT calculations (B3LYP functional, 6-311+G*/LANL2DZ basis sets) supports the vibrational assignments and the identification of these metal carbonyl complexes. The average scale factor for the C−O vibrational modes is 0.971 ± 0.007. This scale factor times the calculated symmetric mode for $Ni(CO)_3$ predicts 2110 cm^{-1}, which is in excellent agreement with the 2100 ± 80 cm^{-1} PES measurement.[20] The uncorrected sequential binding energies of metal carbonyls agree well with the collision-induced dissociation data. The NBO analyses have also been done on all nine monocarbonyls; the only two nonlinear monocarbonyls are $PdCO^-$ and $PtCO^-$.

The PtCO complex observed here in solid neon at 2065 cm^{-1} is just below value for low-coverage top site CO on Pt(111) measured by ELS (258 meV = 2080 cm^{-1}) and very low coverage at 20 K by RAIRS at 2089 cm^{-1}.[43,44] The RhCO and IrCO frequencies in solid neon[37] agreed with the low-coverage top-site measurements within 10 cm^{-1}.

Catalyst systems with Ni(II) have provided carbonyl absorptions in the 2204−2191 cm^{-1} region attributed to Ni(II)−CO on $AlPO_4$, Al_2O_3, and SiO_2 supports.[45] The present observation of $NiCO^+$ at 2206.5 cm^{-1} provides strong evidence that the local charge on these supported Ni(II) catalyst systems is +1.0 and not near the +2.0 implied by the oxidation state. The average CO stretching frequencies of $Pd(CO)_2(SO_3F)_2$ and $Pt(CO)_2(SO_3F)_2$ were reported as 2217 and 2201 cm^{-1}.[46,47] Our observations of neon matrix-isolated $Pd(CO)_2^+$ and $Pt(CO)_2^+$ at 2210.5 and 2210.3 cm^{-1} strongly suggest that the local charge on these solvated dicarbonyls is near +1 instead of +2 that might be inferred from the II oxidation state in their molecular formulas.

Acknowledgment. The authors gratefully acknowledge National Science Foundation support from Grant CHE 97-00116 and a preprint from L. Manceron.

References and Notes

(1) Mond, L.; Langer, C.; Quincke, F. *J. Chem. Soc.* **1890**, 749. Mond, L.; Langer, C. *J. Chem. Soc.* **1891**, 1090.

(2) Cotton, F. A.; Wilkinson, G. *Advanced Inorganic Chemistry*, 5th ed.; Wiley: New York, 1988. Collman, J. P.; Hegedus, L. S.; Norton, J. R.; Finke, R. G. *Principles and Applications of Organotransition Metal Chemistry*; University Science Books: Mill Valley, CA, 1987.

(3) Tolman, C. A. *Chem. Soc. Rev.* **1972**, *1*, 337. Casey, C. P.; Cyr, C. R. *J. Am. Chem. Soc.* **1973**, *95*, 2248. Mitchener, J. C.; Wrighton, M. S. *J. Am. Chem. Soc.* **1981**, *103*, 975. Whetten, R. L.; Fu, K.; Grant, E. R. *J. Am. Chem. Soc.* **1982,** *104*, 4270. Weitz, E. *J. Phys. Chem.* **1987**, *91*, 3945.

(4) Walsh, S. P.; Goddard, W. A., III *J. Am. Chem. Soc.* **1976**, *98*, 7908.

(5) Nekrylova, J. V.; Harrison, I. *J. Chem. Phys.* **1994,** *101*, 1730.

(6) DeKock, R. L. *Inorg. Chem.* **1971**, *10*, 1205. Bach, S. B. H.; Taylor, C. A.; Van Zee, R. J.; Vala, M. T.; Weltner, W., Jr. *J. Am. Chem. Soc.* **1986,** *108*, 7104. Joly, H. A.; Manceron, L. *Chem. Phys.* **1998**, *226*, 61.

(7) Howard, I. A.; Pratt, G. W.; Johnson, K. H.; Dresselhaus, G. *J. Chem. Phys.* **1981**, *74*, 3415. Blomberg, M.; Brandemark, U.; Johanson, J.; Siegbahn, P.; Wennerberg, J. *J. Chem. Phys.* **1988,** *88*, 4324. Blomberg, M.; Siegbahn, P.; Lee, T. J.; Rendell, A. P.; Rice, J. E. *J. Chem. Phys.* **1991,** *95*, 5898. Sodupe, M.; Bauschlicher, C. W., Jr.; Lee, T. J. *Chem. Phys. Lett.* **1992,** *189*, 266.

(8) Kündig, E. P.; Moskovits, M.; Ozin, G. A. *Can. J. Chem.* **1972,** *50*, 3587.

(9) Darling, J. H.; Ogden, J. S. *J. Chem. Soc., Dalton Trans.* **1973,** 1079.

(10) Kündig, E. P.; McIntosh, D.; Moskovits, M.; Ozin, G. A. *J. Am. Chem. Soc.* **1973**, *95*, 7234.

(11) Adamo, C.; Lelj, F. *J. Chem. Phys.* **1995**, *103*, 10605.

(12) Sosa, R. M.; Gardiol, P.; Beltrame, G. *Int. J. Quantum Chem.* **1998**, *69*, 371.

(13) Fournier, R. *J. Chem. Phys.* **1993,** *99*, 1801.

(14) Fournier, R. *J. Chem. Phys.* **1993**, *98*, 8041.

(15) Xu, X.; Lü, X.; Wang, N.; Zhang, Q.; Ehara, M.; Nakatsuji, H. *Int. J. Quantum Chem.* **1999,** *72*, 221.

(16) Pápai, I.; Goursot, A.; St-Amant, A.; Salahub, D. R. *Theor. Chim. Acta* **1992,** *84*, 217.
(17) Basch, H.; Cohen, D. *J. Am. Chem. Soc.* **1983,** *105*, 3856.
(18) Jonas, V.; Thiel, W. *J. Chem. Phys.* **1995**, *102*, 8474.
(19) Jonas, V.; Thiel, W. *J. Phys. Chem. A* **1999,** *103*, 1381.
(20) Stevens, A. E.; Feigerle, C. S.; Lineberger, W. C. *J. Am. Chem. Soc.* **1982**, *104*, 5026.
(21) Klopcic, S. A.; Moravec, V. D.; Jarrold, C. C. *J. Chem. Phys.* **1999**, *110*, 8986.
(22) Sunderlin, L. S.; Wang, D.; Squires, R. R. *J. Am. Chem. Soc.* **1992**, *114*, 2788.
(23) Khan, F. A.; Steele, D. L.; Armentrout, P. B. *J. Phys. Chem.* **1995,** *99*, 7819.
(24) Barnes, L. A.; Rosi, M.; Bauschlicher, C. W., Jr. *J. Chem. Phys.* **1990**, *93*, 609.
(25) Zhou, M.; Andrews, L. *J. Am. Chem. Soc.* **1998,** *120*, 11499. Further work has identified $NiCO^+$ at 2176.3 cm^{-1} in solid argon. See references for previous argon matrix work on $Ni(CO)_n$.
(26) Chertihin, G. V.; Saffel, W.; Yustein, J. T.; Andrews, L. Neurock, M.; Ricca, A.; Bauschlicher, C. W., Jr. *J. Phys. Chem.* **1996,** *100*, 5261.
(27) Andrews, L.; Chertihin, G. V.; Neurock, M. *J. Phys. Chem.* **1995,** *100*, 14609.
(28) Burkholder, T. R.; Andrews, L. *J. Chem. Phys.* **1991**, *95*, 8697.
(29) Hassanzadeh, P.; Andrews, L. *J. Phys. Chem.* **1992,** *96*, 9177.
(30) *Gaussian 94*, Revision B.1; Frisch, M. J.; Trucks, G. W.; Schlegel, H. B.; Gill, P. M. W.; Johnson, B. G.; Robb, M. A.; Cheeseman, J. R.; Keith, T. A.; Petersson, G. A.; Montgomery, J. A.; Raghavachari, K.; Al-Laham, M. A.; Zakrzewski, V. G.; Ortiz, J. V.; Foresman, J. B.; Cioslowki, J.; Stefanov, B. B.; Nanayakkara, A.; Challacombe, M.; Peng, C. Y.; Ayala, P. Y.; Chen, W.; Wong, M. W.; Andres, J. L.; Replogle, E. S.; Gomperts, R.; Martin, R, L.; Fox, D. J.; Binkley, J. S.; Defrees, D. J.; Baker, J.; Stewart, J. P.; Head-Gordon, M.; Gonzalez, C.; Pople, J. A. Gaussian, Inc.: Pittsburgh, PA, 1995.
(31) Lee, C.; Yang, E.; Parr, R. G. *Phys. Rev. B* **1988,** *37*, 785.
(32) McLean, A. D.; Chandler, G. S. *J. Chem. Phys.* **1980**, *72*, 5639. Wachters, A. J. H. *J. Chem. Phys.* **1970**, *52*, 1033. Hay, P. J. *J. Chem. Phys*. **1977,** *66*, 4377. K. Raghavachari, K.; Trucks, G. W. *J. Chem. Phys.* **1989**, *91*, 1062.
(33) Hay, P. J.; Wadt, W. R. *J. Chem. Phys.* **1985**, *82*, 270. Wadt, W. R.; Hay, P. J. *J. Chem. Phys.* **1985,** *82*, 284. Hay, P. J.; Wadt, W. R. *J. Chem. Phys.* **1985**, *82*, 299.
(34) Glendening, E. D.; Reed, A. E.; Carpenter, J. E.; Weinhold, F. *NBO Version 3.1*.
(35) Darling, J. H.; Ogden, J. S. *J. Chem. Soc., Dalton Trans.* **1972,** 2496.
(36) Manceron, L.; Alikhani, M. E. *Chem. Phys.* **1999,** *244*, 215. Manceron, L.; Tremblay, B.; Alikhani, M. E. *J. Phys. Chem. A* **2000**, in press.
(37) Zhou, M.; Andrews, L. *J. Phys. Chem. A* **1999,** *103*, 7773 (Co, Rh, Ir + CO).
(38) Zhou, M.; Andrews, L. *J. Chem. Phys.* **1999,** *110*, 10370 (Fe + CO).
(39) Galbraith, J. M.; Schaefer, H. F. III *J. Chem. Phys.* **1996,** *105*, 862.
(40) Huber, K. P.; Herzberg, G. *Constants of Diatomic Molecules*; Van Nostrand-Reinhold: New York, 1979.
(41) Bytheway, I.; Wong, M. W. *Chem. Phys. Lett.* **1998,** *282*, 219.
(42) Goldman, A. S.; Krogh-Jespersen, K. *J. Am. Chem. Soc.* **1996,** *118*, 12159.
(43) Froitzheim, H.; Hopster, H.; Ibach, H.; Lehwald, S. *Appl. Phys.* **1977,** *13*, 147.
(44) Nekrylova, J. V.; French, C.; Artsynkhovich, A. N.; Ukrainkev, V. A.; Harrison, I. *Surf. Sci. Lett*. **1993,** *295*, L987.
(45) Lindblad, T.; Rebenstorf, B. *Acta Chem. Scand.* **1991,** *45*, 342.
(46) Hwang, G.; Wang, C.; Bodenbinder, M.; Willner, H.; Aubke, F. *J. Fluorine Chem*. **1994**, *66*, 150.
(47) Wang, C.; Willner, H.; Bodenbinder, M.; Batchelor, R. J.; Einstein, F. W. B.; Aubke, F. *Inorg. Chem.* **1994**, *33*, 3521.